International Journal of Fluid Machinery and Systems
Vol. 13, No. 2, April-June 2020
DOI: http://dx.doi.org/10.5293/IJFMS.2020.13.2.302
ISSN (Online): 1882-9554

Original Paper

The Rotor-Stator Interaction Onboard a Low Specific speed Francis Turbine.

Einar Agnalt[1], Bjørn Winther Solemslie[1], Pål-Tore Selbo Storli[1] and Ole Gunnar Dahlhaug[1]

[1]Waterpower Laboratory, Norwegian University of Science and Technology
Alfred Getz v. 4, 7034 Trondheim, Norway,
einar.agnalt@ntnu.no, bjorn.w.solemslie@ntnu.no, pal-tore.storli@ntnu.no, ole.g.dahlhaug@ntnu.no

Abstract

Over the last years, several breakdowns in hydropower plants with low specific speed Francis runners have been reported. One of the main excitation forces in such runners is the pressure fluctuations originating from the rotor stator interaction. In this paper, the rotor-stator interaction has been analyzed utilizing pressure sensors onboard the runner. The pressure sensors were flush mounted in the hub of the runner and the signals were transmitted through a slip-ring system. The measurements have been analyzed relative to the runner angular position by utilizing an angular position sensor mounted to the shaft end. Measurements with different guide vane angle have been compared in order to study the potential flow interaction and the viscous wake effects for the pressure inside the runner. The results from the onboard pressure measurements found that the phase of the guide vane passing pressure seen by the onboard pressure sensors was independent of the guide vane opening. Hence, the potential flow interaction was found to be the dominant effect and no evidence from the viscous wake effect was found on the onboard pressure.

Keywords: Francis turbine, position measurement, pressure measurement, rotor-stator interaction

1. Introduction

In the recent years, multiple new power plants with installed Francis runner have experienced breakdown after few running hours [1]. In low specific speed runners, the rotor stator interaction (RSI) is the main excitation force on the runner [2]. The nature of the rotor stator interaction is well described in the literature and commonly divided into the effect from potential flow interaction and viscous wake interaction [3–6]. The potential flow effect is related to the accelerated flow in the cascade, and the low- and high-pressure side of the guide vanes [7]. The viscous wake effect is the defects in the flow field affecting the velocity distribution at the runner inlet [8]. To distinguish between the effect from the potential pressure and the viscous wake, a resource demanding numerical analysis or optical access to the vaneless space could be required [9].

With higher head and material savings in the runners, the RSI was early known to be the root cause for several blade cracks and breakdowns in Francis turbines and pump turbines [10, 11]. Tanaka et.al [11] used a known relation from the turbomachinery industry [12] to show that the hydraulic interference between a blade and a guide vane caused an excitation of the runner creating a global excitation pattern similar to the pattern of the frequency response of the runner. Measurements utilizing onboard sensors in the runner were performed by Kobro [13], with focus on the pressure fluctuations in the channel but the details in the RSI were not covered. Similar onboard studies were conducted by Zobeiri [14] and Hasmatuchi [15] in a pump turbine. Lewis et.al [16] showed that the use of guide vane jets effected the torque fluctuations in the runner. Possibly, the potential effect was reduced by disturbing the guide vane trailing edge stagnation point. Moreover, numerical studies of the RSI are available [17–21], but the details in the interacting forces from the potential flow effects and the viscous wake are to the authors knowledge only available in the literature for compressible turbomachinery [3].

The current paper presents a method utilizing pressure measurements related to the guide vane angle and the runner angular position. By relating the onboard pressure measurements to the angular position of the runner, more details about the RSI can be found. Due to small angular rotation of the guide vanes, the angular distribution of the potential pressure is expected to be independent of the guide vane angle. The viscous wake interaction is expected to be dependent on the guide vane angle, as the wake follows the slipstream of the guide vane. Detailed knowledge about the driving forces of the RSI phenomena is crucial when designing future runners, avoiding operation at resonance conditions. The objective of the current study is to differentiate the effect from the potential pressure and the viscous wake on the pressure onboard a runner by relating the measurements to the absolute position of the runner.

Received July 01 2018; revised September 06 2018, February 12 2019; accepted for publication December 11 2019:
Review conducted by Minsuk Choi. (Paper number O18031K) Corresponding author: Einar Agnalt, einar.agnalt@ntnu.no

2. Methods

2.1 Experimental setup

The Francis test-rig available at the Waterpower laboratory, Norwegian University of Science and Technology was used for the experimental studies [22]. The Francis test-rig was equipped with all required instruments to conduct model testing according to IEC 60193[23]. The runner in current study were a 1:5.1 scale with dimensionless specific speed of 0.07. The design was based on the Tokke power plant in Norway. The runner in the current study was a bolted design with 15+15 splitter and full-length blades. The number of guide vanes was 28 and the spiral casing was bolted through 14 stay vanes. The draft tube of the test rig was an elbow-type. The Francis turbine in the test-rig is shown in Fig. 1.

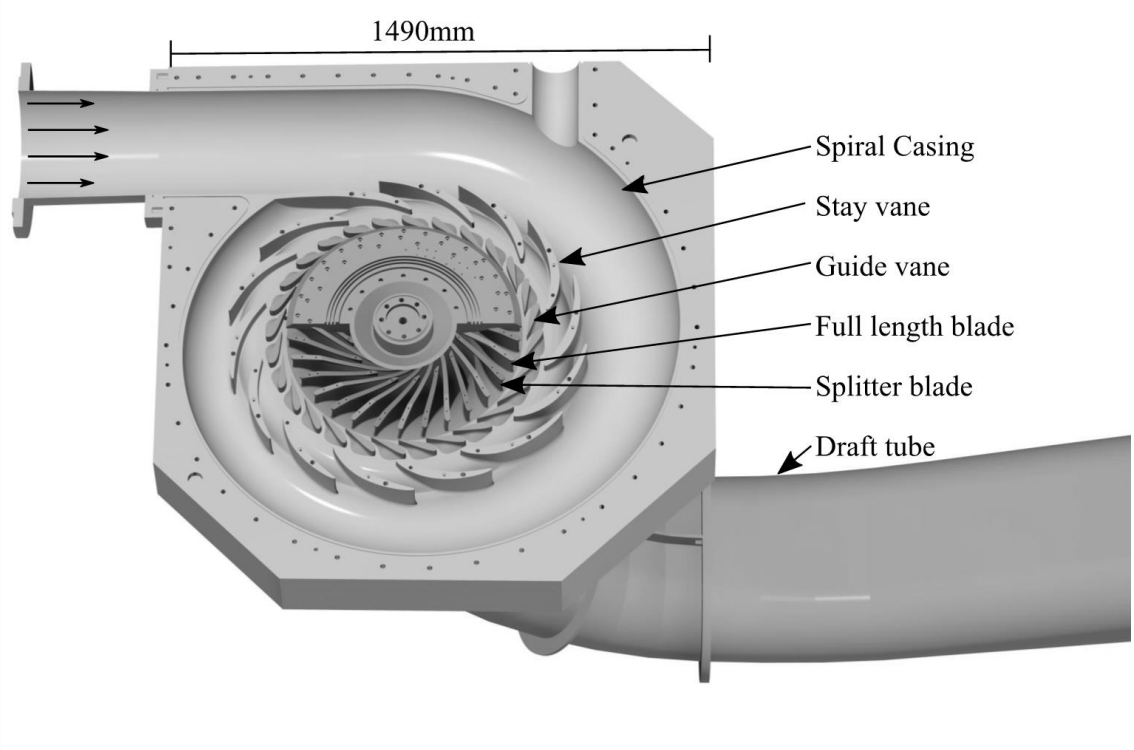

Fig. 1 Three-dimensional view of the investigated Francis turbine.

The pressure from the guide vanes acting on the runner is a result of the upstream flow field and the guide vane cascade design. The center section of the guide vane design is shown in Fig. 2. The figure indicates the free vortex streamlines from the stay vanes. The guide vanes have an angle of attack relative to the free vortex flow, hence lift and circulation is generated creating potential pressure effects [8]. The trailing edge shape is oblique, known to create weak vortices [24].

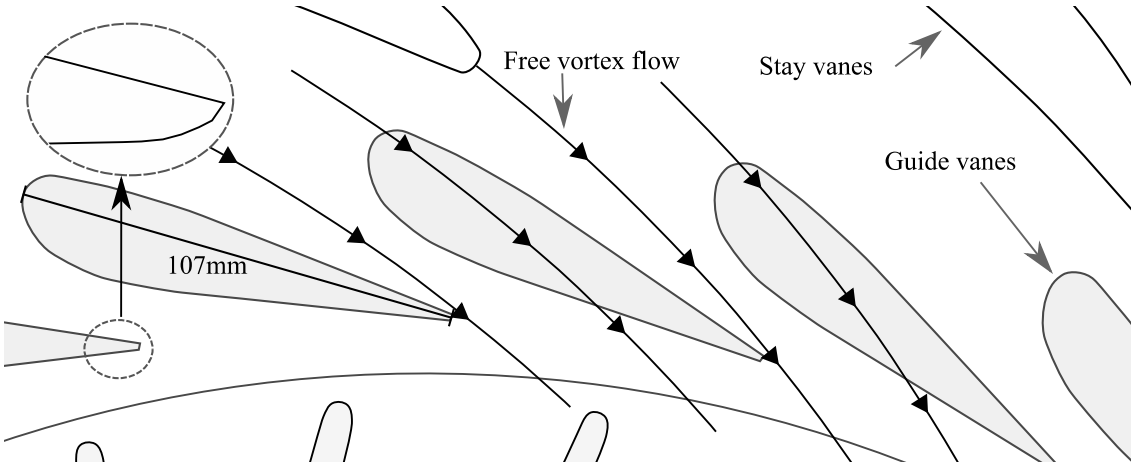

Fig. 2 Guide vane design. The arrows indicate the path described by a free vortex flow. The guide vanes direct the flow creating lift and a pressure field

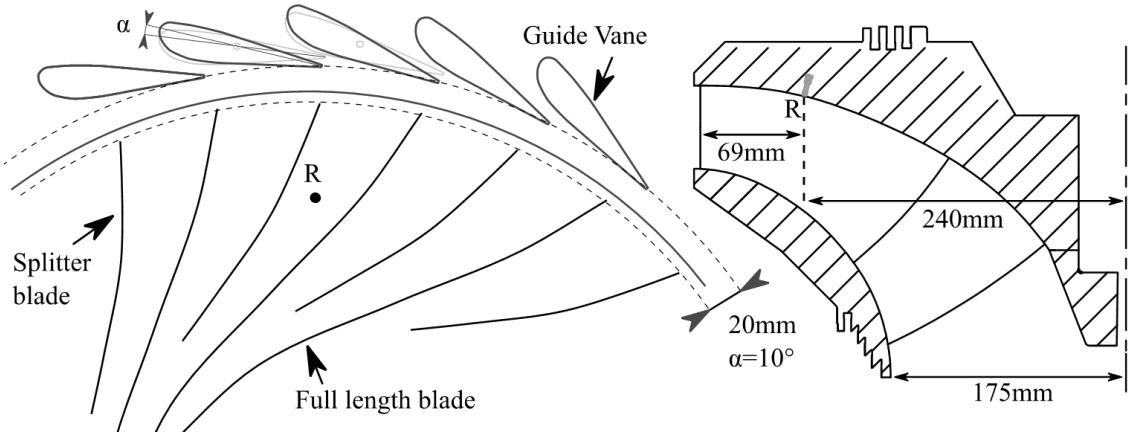

Fig. 3 Onboard pressure sensor R. The sensor is located 69mm radially from the leading edge of the blade. The distance from the trailing edge of the guide vanes to the leading edge of the blades is indicated where α is guide vane opening with 0º as closed position as defined in the IEC60193[23].

Measurements including moving fluids could be severely influenced by the mounting method of the sensor [25]. Recently, pressure sensors with high accuracy and small sizes have become available with flush mounted diaphragm. For application where accurate flush mounting is possible, the uncertainty from mounting i.e. related to hole size, transmission tubes and cavities will be neglectable [26]. The time and frequency response for the measurements is then only related to the dynamic properties of the diaphragm and the data acquisition (DAQ) chain [27]. In the current measurements, flush mounted sensors were selected to reduce uncertainty related to mounting method.

Figure 3 shows the locations of the onboard pressure sensor in the turbine (R). The onboard sensor was mounted in the runner hub. The pressure signal was amplified onboard and then transmitted through a slip-ring before the connection to the DAQ system. A slip-ring was utilized to minimize the time synchronization uncertainty between rotating and stationary domain when relating the pressure to the angular position of the runner.

The position sensor was installed on the end of the shaft, above the generator as shown in Fig. 4. For easier signal analysis and DAQ configuration, the signal was converted to analog +-10V before the DAQ system with a digital to analog converter (DAC).

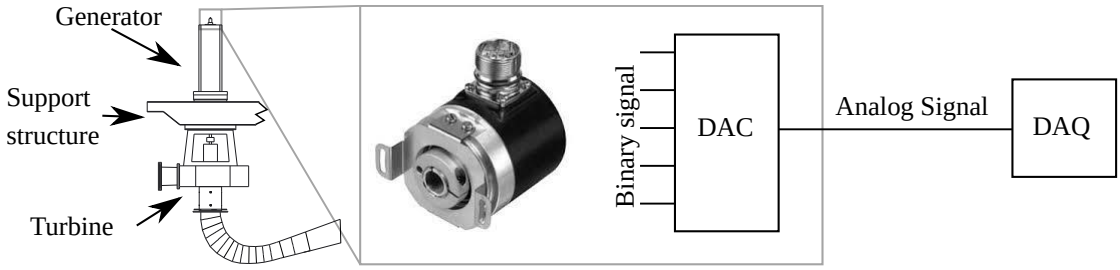

Fig. 4 Position sensor on the shaft

2.2 Measurements

The results in this paper are based on the measurements at three operating points, presented in Table 1.

Table 1. Measurement summary. All parameters are defined according to the IEC60193**[23]**. α is guide vane opening.

Description	n_{ED}	Q_{ED}	Head	α	Speed
Best Efficiency Point (BEP)	0.180	0.154	15.6m	10º	382.7 rpm
Part Load (PL)	0.179	0.107	15.5m	6.7º	379.5 rpm
High Load (HL)	0.179	0.184	15.6m	12.4º	381.9 rpm

2.3 Calibration and uncertainty

Static calibration of the pressure sensors was initially done in an estimated pressure range for the measurements using the guidelines of German Calibration Service [28]. A pneumatic deadweight tester, GE P3000 Series, was used as the primary reference for the pressure calibration. As evaluation of pressure amplitudes is a dynamic quantity, dynamic uncertainty must be addressed. All components in the current pressure measurement chain, from the sensors to the data acquisition, are stated to have resonance frequencies above 10kHz, hence the dynamic uncertainty is assumed to be neglectable and only repeatability and hysteresis from static calibration remain in the uncertainty evaluation. A repeatability test was conducted at 1 Hz with a pressure alternating between 100kPa and 90kPa absolute pressure. The uncertainty budget for the RSI guide vane passing amplitudes at BEP is presented in Table 2.

Table 2. Uncertainty budget for RSI amplitudes, BEP

Sensor	1Hz Repeatability [kPa]	Amplitude RMS of fundamental RSI [kPa]	Relative Uncertainty [%]	Amplitude RMS of first harmonic RSI [kPa]	Relative Uncertainty [%]
R	0.01	1.17	0.85	0.08	13

The uncertainty budget for the position sensor (Z) is summarized in Table 3. The uncertainties are based on given data for the encoder and the DAC. A smoothing filter was utilized to filter the signal noise and the noise uncertainty was calculated from the difference in the raw signal and the filtered position signal used in the analysis. Timing uncertainties were converted to angular offset with the average of the speeds given in Table 1

Table 3. Uncertainty budget of position sensor

Encoder linearity [º]	DAC conversion rate [º]	Noise [º]	Time delay [º]	Total absolute uncertainty [º]
0,05	0	0,4	0,2	0,45

The position accuracy was verified with several measurements at BEP, at different rotational speed and head. The angular shift of the pressure was calculated with cross correlation, and was found to be within the stated total absolute uncertainty.

3. Results

All pressure values presented is calculated as percentage of potential energy (E=gH) and denoted p_E (%) as recommended by the IEC60193[23]. H is net head. Fluctuating quantities are denoted with a tilde (~).

The analysis of the measurands relative to position was done with the use of angular sectors. Sector limits were defined and measurands falling within the limits were added in a sector group. For all values in each sector group, the mean, standard deviation, minimum and maximum were calculated. The process is shown in Fig. 5 where the sector steps are indicated by the minor grid lines. For good visibility of the sectors, the step is set to 2 degrees. In addition to the analysis in Fig. 5, the distribution of values in each sector was calculated. The data was close to normally distributed for all sectors in Fig. 5, hence the variation is believed to be of random nature.

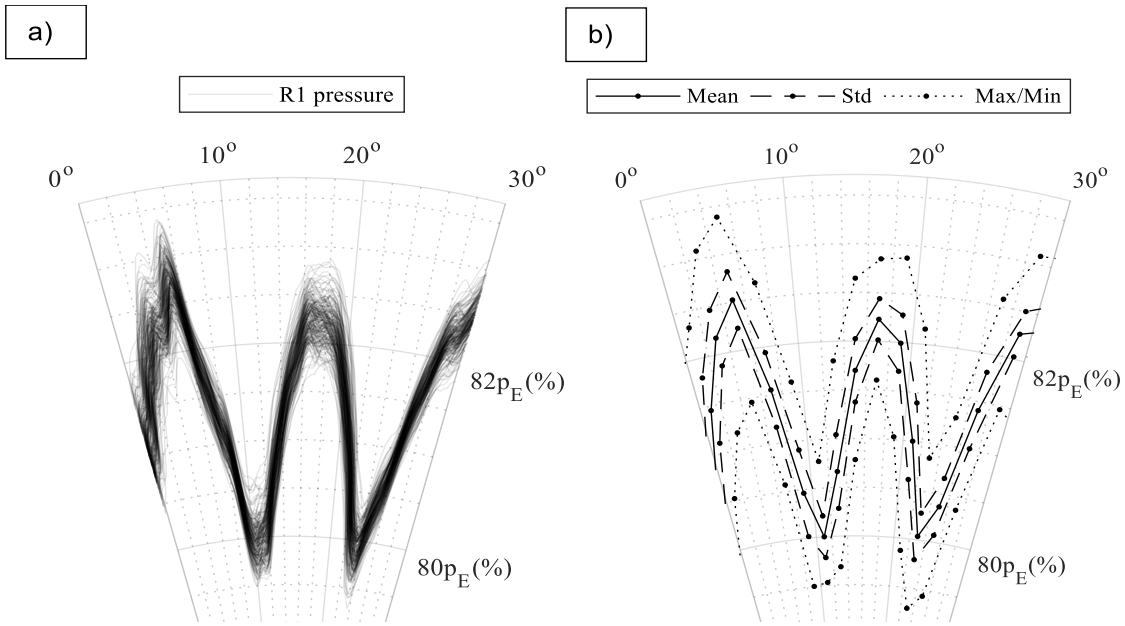

Fig. 5 a) The measured pressure, with sensor R for 180 revolutions of the runner. The plot is made with semi-opaque lines, hence darker color indicates multiple overlapping lines.

b) Calculation in each sector. Mean, standard deviation and maximum/minimum values

The following results were analyzed in sectors for each 0.5 degrees for higher resolution and phase accuracy. In Fig. 6 the mean pressure for each sector is shown for guide vane angle 6.7, 10.0 and 12.4 as presented in Table 1. A high pass filter was used to increase the comparability by removing the low frequency content.

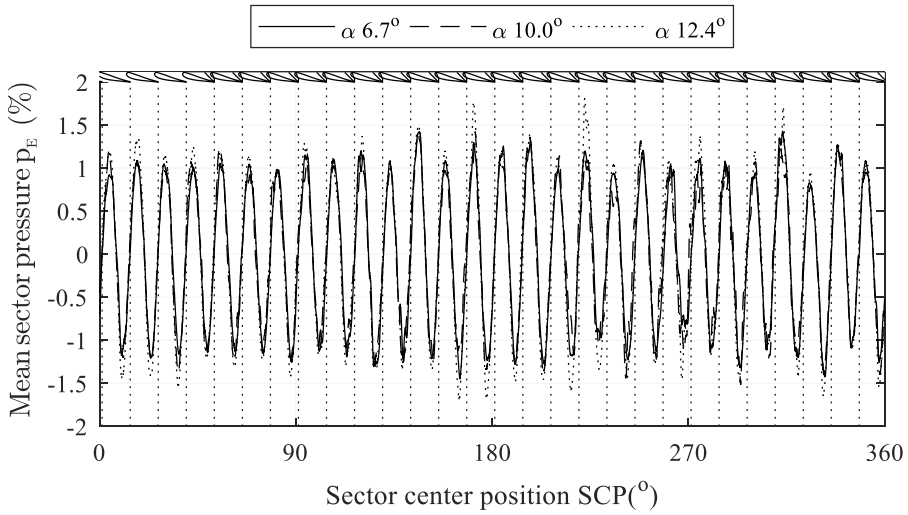

Fig. 6 The mean pressure in the runner for all sectors. The mean is calculated from 180 full revolutions. The vertical dashed lines indicate the distance between the guide vanes

To highlight the details, the sectors from 0º to 40º is shown in Fig. 7.

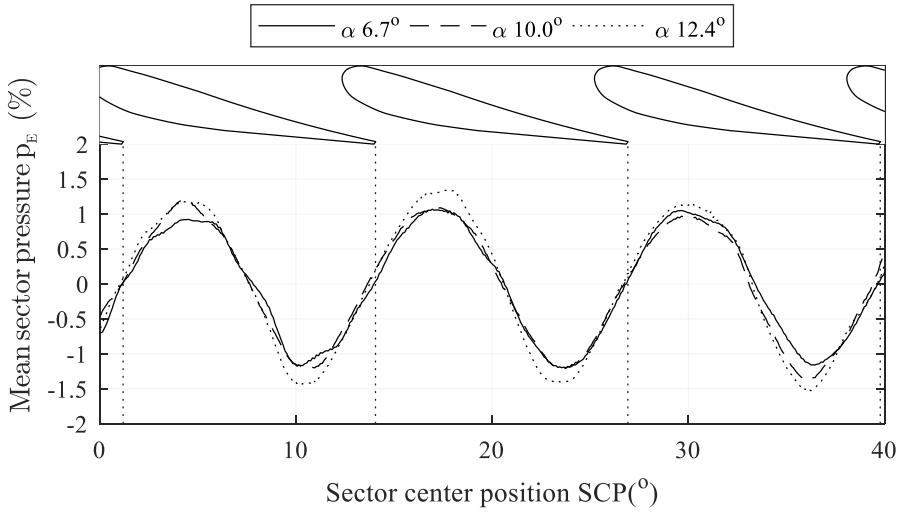

Fig. 7 The mean pressure for the sectors in the range 0º to 40º. The mean is calculated from 180 full revolutions. The vertical dashed lines indicate the distance between the guide vanes trailing edges.

Further details of the measured amplitudes were analyzed with the use of short time fast Fourier transform. The analysis was performed with window length equal to 100 periods of the RSI signal and with 50% overlap. The main component of the presented measurement in Fig. 7 is the fundamental of the guide vane passing pressure. In Fig. 8, the amplitudes of the guide vane passing pressure is shown. The uncertainty bars represent the 95% probability.

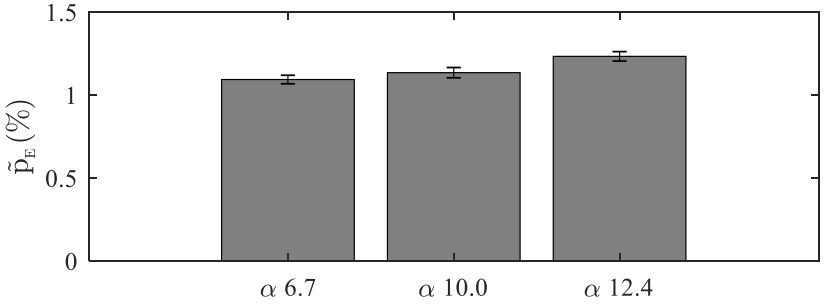

Fig. 8 The fundamental guide vane passing pressure amplitude with 95% probability for the sensor R. The amplitude is percentage of head.

4. Discussion

The analysis of the rotor stator interaction onboard the runner was carried out by analyzing the pressure in one runner channel measured with pressure sensor R. Three guide vane opening angles were investigated to analyze the pressure. It was expected to find a phase shift between the measurements with different guide vane opening relative to the runner position if the viscous wake was the main source for the pressure in the channel as illustrated in Fig. 9. With increasing guide vane opening, the pressure should have a recognizable phase shift against the rotational direction of the runner. Also, from classical wake theory, the pressure amplitudes were expected to be lower since the viscous wake was expected to be weaker on lower guide vane openings, due to longer distance from the trailing edge of the guide vane to the impact point and lower flow velocity [29]. Contrarily, with larger guide vane openings, the wake was directed more on the runner, and the pressure effect from the viscous wake was expected to be more visible.

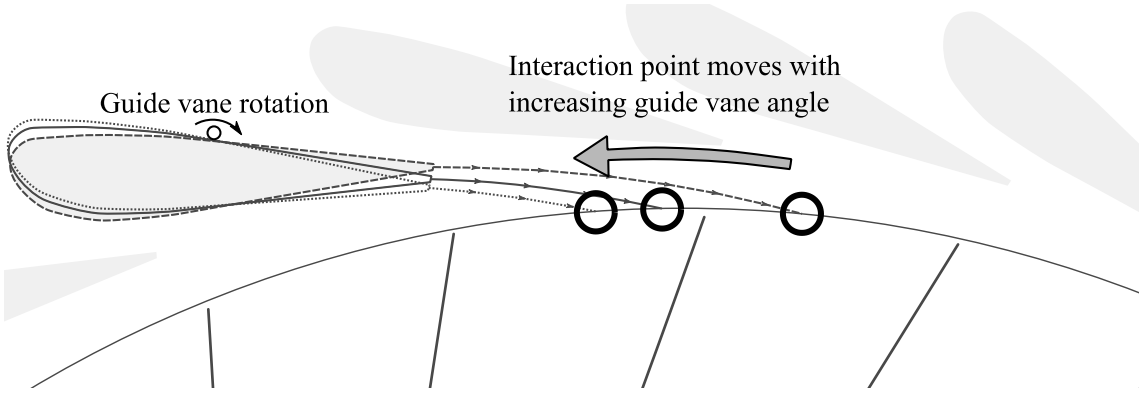

Fig. 9 The viscous wake interaction-point with the runner.
The interaction point is expected to be dependent on the angular position of the guide vane.
The indicated wake is assumed to follow a path described by a free vortex flow.

The dependency of the potential pressure to the guide vane angle was assumed neglectable compared to the viscous wake angular dependency. Due to the Kutta condition, the stagnation point will be located at the trailing edge for all measurements [30], and the trailing edge tangential movement around the runner is in the order of millimeters. At the outlet of the guide vane cascade, the expected pressure field is illustrated in Fig. 10a. High-pressure zones are located around the trailing edge stagnation points. The angular position of the runner in Fig. 10b illustrates the runner position when the channel with the sensor R is most effected by the high-pressure zone. This corresponds to the position were the guide vane trailing edge stagnation point is in the middle of the channel.

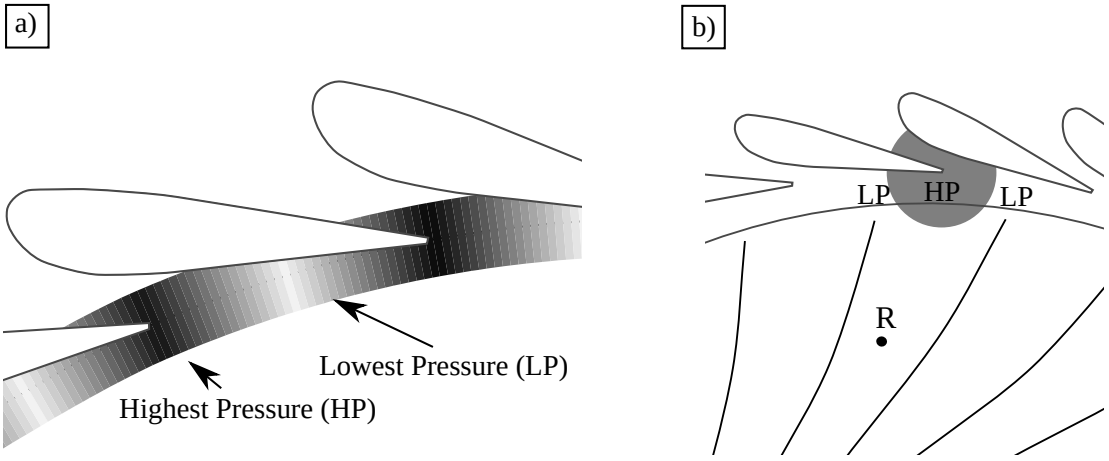

Fig. 10 a) Illustration of the potential pressure at the outlet of the guide vane cascade. b) The angular position of one runner channel relative to the guide vanes Where the effect from potential pressure is expected to be at maximum.

With increasing guide vane angle, the potential pressure effect was expected to give higher pressure fluctuations in the runner, because the gap between the guide vanes to the runner was reduced, and because the strength of the pressure field was expected to increase due to higher flow. On the other hand, a decreasing factor was a possible reduction in the lift force since the guide vanes were more aligned with the free vortex flow from the stay vanes with increasing guide vane opening, as shown in Fig. 2. From the amplitude analysis shown in Fig. 8, there was an increasing trend in amplitude with increasing guide vane opening indicating the influence of the increasing factors.

From the results presented in Fig. 6 and Fig. 7, there is no evidence of a significant phase shift for the pressure in the runner channel relative to position. From the previous discussion about viscous wakes dependency of the guide vane angle and the expected phase shift in the pressure, no evidence of the viscous wake effect in the runner pressure is found. By comparing the assumed

position of the highest-pressure influence from the potential pressure shown in Fig. 10b and the measured pressure shown in Fig. 7, it is clear that the potential pressure is the source for the pressure fluctuations in the runner channel. However, the RSI is highly dependent on the guide vane cascade design and flow conditions [31]. Hence, different lift conditions in the guide vane section and less favorable trailing edge design of the guide vanes will create different results.

5. Conclusion

Analysis of the influence from potential pressure and the viscous wake was done by varying the guide vane angle, hence moving the interaction point of the viscous wake on the runner. The pressure in the runner channel was monitored with a pressure sensor mounted in the runner hub. The analysis of the measurements did not find any phase shift in the pressure relative to the runner position for the investigated guide vane openings. Hence, the pressure in the runner was found to be highly dependent on the potential pressure in the guide vane cascade and there is no clear evidence of any effect on the pressure in the runner channel from the viscous wake. As the geometry in current study is open and available [32], the results could be used for numerical verification. The presented experimental method should be repeated for several designs with a large head range preferably on prototypes for validation.

Acknowledgments

This work was founded by Energy Norway, Norwegian Research Council and the Norwegian Hydropower Center. The authors are grateful for all the support from the technical staff at the Waterpower laboratory which were invaluable to make the measurements possible.

Nomenclature

α	Guide vane opening [°]	$\widetilde{p_E}$	Fluctuating pressure (%)
n_{ED}	Dimensionless speed factor [-]	Q_{ED}	Dimensionless discharge [-]

References

[1] Østby, P. T. K., Billdal, J. T., Sivertsen, K., Haugen, B., and Dahlhaug, O. G., 2016, "Dynamic Stresses In High Head Francis Turbines," Hydropower & Dams, no. 3.
[2] Seidel, U., Hübner, B., Löfflad, J., and Faigle, P., 2012, "Evaluation of RSI-induced stresses in Francis runners," IOP Conference Series: Earth and Environmental Science, vol. 15, no. 5, p. 052010.
[3] Gallus, H. E., Lambertz, J., and Wallmann, T., 1980, "Blade-Row Interaction in an Axial-Flow Subsonic Compressor Stage," J. Eng. Power, vol. 102, no. 1, pp. 169–177.
[4] D. Y. Li, R. Z. Gong, H. J. Wang, X. Z. Wei, Z. S. Liu, and D. Q. Qin, 2016, "Analysis of Rotor-Stator Interaction in Turbine Mode of a Pump-Turbine Model," Journal of Applied Fluid Mechanics, vol. 9, no. 5, pp. 2559–2568.
[5] Arndt, N., Acosta, A., Brennen, C. E., and Caughey, T. K., 1989, "Rotor-stator interaction in a diffuser pump," ASME Journal of Turbomachinery, vol. 111, pp. 213–221.
[6] Dring, R. P., Joslyn, H. D., Hardin, L. W., and Wagner, J. H., 1982, "Turbine Rotor-Stator Interaction," J. Eng. Power, vol. 104, no. 4, pp. 729–742.
[7] Østby, P. T. K., Billdal, J. T., Haugen, B., and Dahlhaug, O. G., 2017, "On the relation between friction losses and pressure pulsations caused by Rotor Stator interaction on the Francis-99 turbine," J. Phys.: Conf. Ser., vol. 782, no. 1, p. 012010.
[8] Antonsen, Ø., 2007, "Unsteady flow in wicket gate and runner with focus on static and dynamic load on runner," Doctoral Thesis, Norwegian University of Science and Technology, Trondheim, Norway.
[9] Gagnon, J.-M., Ciocan, G. D., Deschenes, C., and Iliescu, M., 2008, "Numerical and Experimental Investigation of Rotor-Stator Interactions in an Axial Turbine: Numerical Interface Assessment," in Proceedings of FEDSM2008, Jacksonville, Florida USA, pp. 929–935.
[10] Brekke, H., "A Review on Oscillatory Problems in Francis Turbine," in New Trends in Technologies: Devices, Computer, Communication and Industrial Systems, 2010, InTech.
[11] Tanaka, H., 2011, "Vibration Behavior and Dynamic Stress of Runners of Very High Head Reversible Pump-turbines," International Journal of Fluid Machinery and Systems, vol. 4, no. 2, pp. 289–306.
[12] Tyler, J. M. and Sofrin, T. G., 1962, "Axial Flow Compressor Noise Studies," SAE International, Warrendale, PA, 620532.
[13] Kobro, E., 2010, "Measurement of Pressure Pulsations in Francis Turbines," Doctoral Thesis, Norwegian University of Science and Technology, Trondheim, Norway.

[14] Zobeiri, A., 2009, “Investigations of Time Dependent Flow Phenomena in a Turbine and Pump-Turbine of Francis Type: Rotor-Stator Interactions and Precessing Vortex Rope,” EPFL, Lausanne.
[15] Hasmatuchi, V., 2012, “Hydrodynamics of a pump-turbine operating at off-design conditions in generating mode,” Doctoral Thesis, Ecode Polytechnique Federale de Lausanne, Lausanne, Switzerland.
[16] Lewis, B. J., Cimbala, J. M., and Wouden, A. M., 2012, “Investigation of distributor vane jets to decrease the unsteady load on hydro turbine runner blades,” IOP Conf. Ser.: Earth Environ. Sci., vol. 15, no. 2, p. 022006.
[17] Li, Z., Wang, Z., Wei, X., and Qin, D., 2016, “Flow Similarity in the Rotor–Stator Interaction Affected Region in Prototype and Model Francis Pump-Turbines in Generating Mode,” J. Fluids Eng, vol. 138, no. 6, pp. 061201–061201.
[18] Yan, J., Koutnik, J., Seidel, U., and Hübner, B., 2010, “Compressible simulation of rotor-stator interaction in pump-turbines,” IOP Conference Series: Earth and Environmental Science, vol. 12, p. 012008.
[19] Yonezawa, K., Toyahara, S., Motoki, S., Tanaka, H., Doerfler, P., and Tsujimoto, Y., 2014, “Phase Resonance in Centrifugal Fluid Machinery,” IJFMS, vol. 7, no. 2, pp. 42–53.
[20] Xia, L., Cheng, Y., and Cai, F., 2017, “Pressure Pulsation Characteristics of a Model Pump-turbine Operating in the S-shaped Region: CFD Simulations,” IJFMS, vol. 10, no. 3, pp. 287–295.
[21] Yan, J., Koutnik, J., Seidel, U., and Hübner, B., 2010, “Compressible Simulation of Rotor-Stator Interaction in Pump-Turbines,” IJFMS, vol. 3, no. 4, pp. 315–323.
[22] Trivedi, C., Agnalt, E., and Dahlhaug, O. G., 2018, “Experimental study of a Francis turbine under variable-speed and discharge conditions,” Renewable Energy, vol. 119, pp. 447–458.
[23] IEC, 1999, “NEK IEC 60193 Hydraulic turbines, storage pumps and pump-turbines Model acceptance tests.”
[24] Zobeiri, A., Ausoni, P., Avellan, F., and Farhat, M., 2012, “How oblique trailing edge of a hydrofoil reduces the vortex-induced vibration,” Journal of Fluids and Structures, vol. 32, pp. 78–89.
[25] Rayle, R. E., 1949, “An investigation of the influence of orifice geometry on static pressure measurements,” Master Thesis, Massachusetts Institute of Technology, Cambridge, Massachusetts, USA.
[26] Franklin, R. e. and Wallace, J. M., 1970, “Absolute measurements of static-hole error using flush transducers,” Journal of Fluid Mechanics, vol. 42, no. 01, pp. 33–48.
[27] Hessling, J. P., 2006, “A novel method of estimating dynamic measurement errors,” Measurement Science and Technology, vol. 17, no. 10, p. 2740.
[28] Physikalisch-Technische Bundesanstalt (PTB) and German Calibration Service (DKD), “Guideline DKD-R 6-1 Calibration of Pressure Gauges.” Mar-2014.
[29] White, F. M., 2005, Viscous Fluid Flow, 3 edition. New York, NY: McGraw-Hill Education.
[30] White, F., 2015, Fluid Mechanics, 8 edition. New York, NY: McGraw-Hill Education.
[31] Thapa, B. S., Trivedi, C., and Dahlhaug, O. G., 2016, “Design and development of guide vane cascade for a low speed number Francis turbine,” Journal of Hydrodynamics, Ser. B, vol. 28, no. 4, pp. 676–689.
[32] “Francis-99 NTNU.” [Online]. Available: https://www.ntnu.edu/nvks/francis-99. [Accessed: 10-Sep-2018].